Received: 10 October 2017 | Revised: 8 January 2018 | Accepted: 22 January 2018

DOI: 10.1002/nbm.3907

RESEARCH ARTICLE

WILEY NMR IN BIOMEDICINE

Cranial irradiation increases tumor growth in experimental breast cancer brain metastasis

Amanda M. Hamilton[1] | Suzanne M. Wong[1] | Eugene Wong[2,3] | Paula J. Foster[1,2]

[1] Robarts Research Institute, Imaging Research Laboratories, University of Western Ontario, London, ON, Canada

[2] Department of Medical Biophysics, Western University, London, ON, Canada

[3] Department of Physics and Astronomy, Western University, London, ON, Canada

Correspondence
A. M. Hamilton, Robarts Research Institute, Imaging Research Laboratories, University of Western Ontario, London, ON, Canada.
Email: hamilton@robarts.ca

Funding information
Brain Tumour Foundation of Canada; Brain Tumour Foundation of Canada; Canadian Institutes of Health Research

Whole-brain radiotherapy is the standard of care for patients with breast cancer with multiple brain metastases and, although this treatment has been essential in the management of existing brain tumors, there are many known negative consequences associated with the irradiation of normal brain tissue. In our study, we used *in vivo* magnetic resonance imaging analysis to investigate the influence of radiotherapy-induced damage of healthy brain on the arrest and growth of metastatic breast cancer cells in a mouse model of breast cancer brain metastasis. We observed that irradiated, but otherwise healthy, neural tissue had an increased propensity to support metastatic growth compared with never-irradiated controls. The elucidation of the impact of irradiation on normal neural tissue could have implications in clinical patient management, particularly in patients with residual systemic disease or with residual radio-resistant brain cancer.

KEYWORDS

breast cancer brain metastasis, experimental mouse model, MRI, radiotherapy

1 | INTRODUCTION

As therapies that control cancers outside of the brain improve, patients are surviving for longer and the incidence of metastasis to sanctuary sites, such as the brain, is observed more frequently.[1] The management of patients with brain metastases from breast cancer continues to be a significant clinical challenge. Of particular concern is the treatment of brain metastases in patients with triple negative breast cancer (TNBC). Clinically, 70% of patients with TNBC respond well to treatment, but, unfortunately, in 30% of patients, recurrence occurs within the first 3 years post-treatment and, in these cases, cure is unlikely. TNBC is unresponsive to hormone therapy, has a high incidence of brain metastasis and has the shortest (approximately 4 months) median overall survival after brain tumor development compared with other subtypes of breast cancer.[2,3]

Whole-brain radiotherapy (RT) is the standard treatment for patients with breast cancer with more than three brain metastases, and has been shown to be essential in multiple tumor management. In this scenario, the healthy brain tissue receives significant doses of radiation; unfortunately, RT is known to have multiple negative consequences in normal brain tissue, including radio-necrosis (tissue death), cognitive deficits and both short- and long-term inflammation.[4] The neuro-inflammatory response to RT results in the up-regulation of multiple inflammatory mediators and the infiltration of immune cells from outside the brain.[4,5] Although several immune cells serve roles in immunity against cancer, others have been implicated in tumor progression and metastasis with established roles in tumor-associated blood vessel formation and tissue remodeling, as well as tumor cell motility, in and out of blood vessels.[6]

Several studies have suggested that RT might promote the invasiveness of cancer cells.[7-13] For example, a study by Bouchard et al.[13] showed that RT of normal mouse mammary tissue increased the migration of mammary cancer cells from the contralateral mammary fat pad, and also increased the number of circulating cancer cells and the incidence of lung metastases. In the current study, we investigated the influence of radiation-induced damage on the arrest and growth of metastatic breast cancer cells in the brain using an immune-competent mouse model of TNBC.

Abbreviations used: 231BR, MDA-MB231BR human brain tropic breast cancer metastatic cell line; 3-D bSSFP, three-dimensional balanced steady-state free precession; 4T1-BR5, murine brain tropic breast cancer metastatic cell line; BBB, blood–brain barrier; bSSFP, balanced steady-state free precession; COX-2, cyclooxygenase-2; DAB, 3,3′-diaminobenzidine; DMEM, Dulbecco's modified Eagle medium; FBS, fetal bovine serum; ICAM-1, intercellular adhesion molecule-1; IgG, immunoglobulin G; IHC, immunohistochemistry; IL6, interleukin 6; IO, iron oxide nanoparticles; MHC II, major histocompatibility complex class 2; MRI, magnetic resonance imaging; PPB, Perls Prussian blue; RT, whole-brain radiotherapy; SEM, standard error of the mean; TE, echo time; TNBC, triple negative breast cancer; TNFα, tumor necrosis factor alpha; TR, repetition time

To aid this investigation, we employed the use of cellular magnetic resonance imaging (MRI) techniques that enable the study of brain metastasis development longitudinally with high spatial resolution, good tumor to normal tissue contrast and single-cell sensitivity.[14-19] A key aspect of this study was our ability to use iron cell labeling and MRI to track initial cancer cell arrest, as well as tumor progression, over time. This approach could not be successfully conducted with traditional histological methods. Endpoint histology was pivotal in our initial investigation of the differential expression of pathological markers in tumors arising in pre-irradiated or normal neural tissue.

2 | MATERIALS AND METHODS

2.1 | Ethical statement

This study was carried out in strict accordance with the standards of the Canadian Council of Animal Care. All animal work was approved by the Animal Use Subcommittee of the University Council on Animal Care at the University of Western Ontario. All efforts were made to minimize any suffering, and mice were humanely euthanized following the experiments.

2.2 | Cell culture

Murine brain tropic breast cancer cells (4T1-BR5) were a kind gift from Dr Patricia Steeg's laboratory at the National Cancer Institute (Bethesda, MA, USA).[20-22] Cells were grown in Dulbecco's modified Eagle medium (DMEM) supplemented with 10% fetal bovine serum (FBS), 100 IU/mL penicillin and 100 μg/mL streptomycin. For tracking cell delivery, cells were labeled with iron oxide nanoparticles (IO; 0.9 μm, labeled with Flash Red; Bangs Laboratory, Fishers, IN, USA), as described previously.[14] Labeled cells underwent sequential washing before and after dissociation prior to injection into animals, as described later. Prior to injection, cell viability was assessed on a subset of cells using the trypan blue exclusion assay. The efficiency of cell labeling was also assessed by Perl's Prussian blue (PPB) staining, as described previously.[23]

2.3 | Animals

Female BALB/c mice were acquired at 6–8 weeks from Charles River Laboratories (product code #028; Wilmington, MA, USA) and were housed in dedicated animal housing. All RT treatments, cell delivery and imaging procedures were performed under inhalant anesthesia using 1–2% isoflurane in 100% oxygen. Mice were monitored by weight and visual inspection for any signs of stress or severe illness until endpoint.

2.4 | Whole-brain irradiation

A radiation treatment plan of a dose of 10 Gy in one fraction to the whole mouse brain was delivered 7 days prior to cell delivery. The dose and time frame were chosen on the basis of a previously published study of the effect of brain irradiation on normal brain in an immune-competent mouse strain.[5] Radiation delivery was performed using an in-house custom micro-irradiation system (140 kVp, 50 kW) with on-board image guidance.[24] Anesthetized mice were placed in the tail-first prone position and the skull was located using on-board fluoroscopy. Computerized collimators were positioned to create a 10 × 14-mm^2 field that encompassed the brain and shielded the remainder of the mouse head and body. The whole brain was irradiated using two equal-weighted, parallel-opposed beams for a cumulative dose of 10 Gy, as described and validated previously.[18,24] All irradiated mice received their full 10-Gy dose and no irradiated mice showed any outward sign of adverse effects caused by the irradiation treatment. Control mice were handled and anesthetized, but received no RT.

2.5 | Ultrasound-guided cell delivery

Vevo MicroMarker microbubble solution (Fujifilm VisualSonics Inc., Toronto, ON, Canada) was reconstituted according to the manufacturer's instructions. For each cell injection, 2×10^4 iron-labeled 4T1-BR5 cells were resuspended in 100 μL of sterile saline containing 15% microbubble solution (with a final concentration of 3×10^7 microbubbles per injection). Anesthetized mice were secured to a heated physiological monitoring platform (THM-150; VisualSonics Inc.) with a platform temperature maintained at approximately 37°C. Chest fur was removed using depilation cream (Nair, Church & Dwight Company Inc., Princeton, NJ, USA) and ultrasound coupling gel was applied. All ultrasound imaging was performed using a Vevo 2100 high-frequency imaging system (VisualSonics, Inc.) equipped with a 256-element linear array transducer (MS-250) transmitted at 18 MHz in non-linear contrast mode. The cell suspension was loaded into a 100-μL Hamilton syringe equipped with a 30G needle. Ultrasound was used to guide the needle through the chest wall and directly into the left ventricle. Cells were delivered over a 20-s time period and successful injection was indicated by microbubble contrast enhancement in the blood volume of the left ventricle. The mice were monitored until awake and fully active.

2.6 | MRI and analysis

All MRI was performed on a 3-T GE Discovery MR750 whole-body MR scanner using a custom-built high-performance gradient coil (maximum gradient strength, 500 mT/m; peak slew rate, 3000 T/m/s). Brain imaging was achieved using a custom solenoid radiofrequency coil (inner

diameter, 1.5 cm) and a three-dimensional balanced steady-state free precession (3-D bSSFP) sequence. To confirm and quantify cell delivery to the brain, anesthetized mice were imaged on the day of cell injection using the following parameters: resolution, 100 × 100 × 200 μm^3 (slice thickness of 200 μm in the rostral/caudal direction); repetition time/echo time (TR/TE) = 8/4 ms; flip angle, 35°; bandwidth, ±42 kHz; four phase cycles; scan time, 14 min.[25] Only mice with evident signal voids in the brain (representing successfully delivered IO-labeled cancer cells) were continued in the study and imaged again at endpoint (13 days after cell injection) to assess tumor growth. Endpoint imaging was conducted using the following parameters: resolution, 100 × 100 × 200 μm^3; TR/TE = 10/5 ms; flip angle, 35°; bandwidth, ±12.5 kHz; eight phase cycles; number of excitations, two; scan time, 36 min.[19]

All images were analyzed by two blind observers using the open-source DICOM viewer OsiriX (Pixemo, Bernex, Switzerland). Signal voids were manually counted in cell delivery MR images. Endpoint MR images were assessed for the number of MR-detectable tumors, average tumor volume and total tumor burden (tumor volume across the entire mouse brain). Tumor boundaries on each slice were manually traced and volumes were determined using a volume calculation algorithm in OsiriX. All MR data was averaged between observers, summarized for each individual mouse and summary data were compared across conditions.

2.7 | Euthanasia and tissue processing

Animals were sacrificed after endpoint MRI by isoflurane overdose. After sacrifice, mice were perfused with 0.9% saline solution, followed by 10% formalin. Brains were excised and immersion fixed for 24 h in 10% formalin before undergoing cryoprotection through immersion in increasing concentrations of sucrose (10–30%). Fixed cryoprotected mouse brains were frozen embedded in O.C.T. Compound (Tissue-Tek, Sakura Finetek Europe B.V., Leiden, the Netherlands) and sectioned at 10 μm.

2.8 | Histology and immunohistochemistry (IHC)

Select tissue sections were used to perform IHC for markers galectin-3 (1: 50, clone: eBioM3/38; Thermo Fisher Scientific, Burlington, ON, Canada), intercellular adhesion molecule-1 (1: 50, ICAM-1/CD54, clone: eBioKAT-1; Thermo Fisher Scientific), Ki67 (1: 400, ab15580; abcam Inc., Toronto, ON, Canada) and F4/80 (1: 400, clone: CI:A3-1, MCA497F; BioRad AbD Serotec, Raleigh, NC, USA). After a 1-h primary antibody incubation, species-appropriate biotinylated secondary antibodies (1: 300, 30 min incubation; Vector Laboratories Canada Inc., Burlington, ON, Canada) were used, followed by a 30-min incubation with a horseradish peroxidase–streptavidin complex (1: 300, prod no. 405210; Biolegend, Inc., San Diego, CA, USA) and DAB peroxidase substrate kit (3,3′-diaminobenzidine; 2–8-min incubation depending on the primary antibody used, SK-4100; Vector Laboratories Canada Inc.) according to the manufacturer's instructions. Three 5-min washes were performed between each of the antibody and reagent steps. All IHC stained sections were counterstained with Harris hematoxylin before cover-slipping. IHC microscopy was performed using a Zeiss AXIO Imager (Carl Zeiss Canada Ltd., North York, ON, Canada).

To assess the percentage staining area, color IHC images underwent color deconvolution using ImageJ open source image processing software (Fiji version 2.0.0-rc-54/1.51 h, National Institutes of Health, Rockville, MD, USA). Tissue samples from each of the imaged mice were used for the IHC assessments. A total of 100–120 regions of interest were assessed per treatment group per IHC stain. All 'color 2' DAB channels for the individual section images were thresholded to the same value and the threshold area fraction was measured. To assess percentage positive staining for Ki67 IHC staining, DAB-positive nuclei were counted using the cell counter plugin on the ImageJ platform (Fiji version 2.0.0-rc-54/1.51 h) and compared with the total number of counted nuclei (DAB staining plus hematoxylin-counterstained nuclei). All tissue section image analysis data were compared across conditions, and averages and measures of error are reported.

2.9 | Statistical analysis

All statistical analysis was performed using unpaired Student *t*-tests in GraphPad Prism software (Version 7.0a; GraphPad Software, Inc., La Jolla, CA, USA). All graphed data are presented as the mean with standard error of the mean (SEM) (*$p < 0.05$, **$p < 0.01$, ***$p < 0.001$, ****$p < 0.0001$).

3 | RESULTS

3.1 | Detection of cell delivery and metastatic growth

4T1-BR5 cells readily took-up iron particles and exhibited a >90% labeling efficiency, as determined by PPB staining (data not shown). Iron labeling did not have a discernible effect on cell viability as measured by trypan blue exclusion assay (>90% viable with or without cell labeling). MRI was used to verify and quantify the successful delivery of iron-labeled cells to the brain parenchyma of control or RT brains following ultrasound-guided intracardiac injection. The bSSFP imaging sequence used permitted the detection of the iron-containing cancer cells as signal voids in MR images. Representative MR images of successful delivery to a control and an RT mouse brain are shown in Figure 1A,B, respectively. Seven of eight control mice and all injected irradiated mice (eight of eight) exhibited successful whole-brain seeding of cells and were assessed for the duration of the study. There was no statistically significant difference in the delivery of cells between the experimental conditions ($p = 0.95$; Figure 1C).

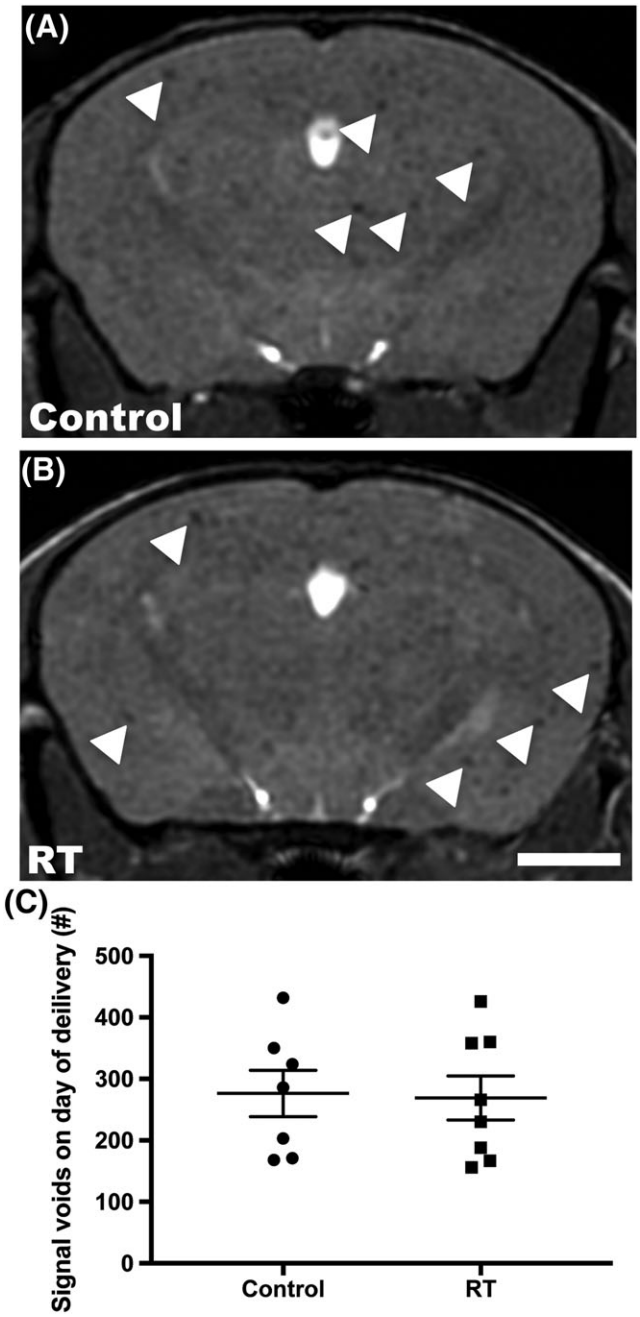

FIGURE 1 Visualization of the delivery of iron-labeled 4T1-BR5 cells by balanced steady-state free precession (bSSFP) magnetic resonance imaging (MRI). Representative axial MR images of control A, and pre-irradiated RT; B, mouse brains on the day of intracardiac cell injection with 2×10^4 iron nanoparticle-labeled 4T1-BR5 cells. White arrowheads indicate examples of signal voids. Scale bar, 2 mm. Statistically equivalent (p = 0.889) cell delivery was detected in the mouse brain irrespective of condition C. Analyzed by Student's unpaired two-tailed t-test

3.2 | Effect of pre-irradiation on brain tumor growth

Metastasis development from injected 4T1-BR5 breast cancer cells in mouse brain pre-irradiated with 10 Gy, 7 days prior to cell delivery, was compared with that of never-irradiated controls. At endpoint, metastases appeared as high-signal intensity regions in bSSFP images relative to the normal brain parenchyma, as observed in previous assessments.[19] Representative images of control and RT mouse brains at endpoint are shown in Figure 2A,B, respectively. Image analysis revealed a significant difference in the observed number (Figure 2C, p = 0.001) of detectable brain tumors in pre-irradiated (RT) mouse brains compared with never-irradiated controls, with 32.0 ± 2.5 and 18.5 ± 2.1 metastases detected, respectively. The RT group also displayed a significantly greater average tumor volume (0.28 ± 0.03 mm^3) than the control mouse brains (0.20 ± 0.01 mm^3, p = 0.01, Figure 2D). Subsequently, these two distinct differences in tumor progression resulted in a very significant difference (p = 0.0002, Figure 2E) in total tumor burden between experimental groups (control, 2.93 ± 0.21 mm^3; RT, 5.16 ± 0.99 mm^3).

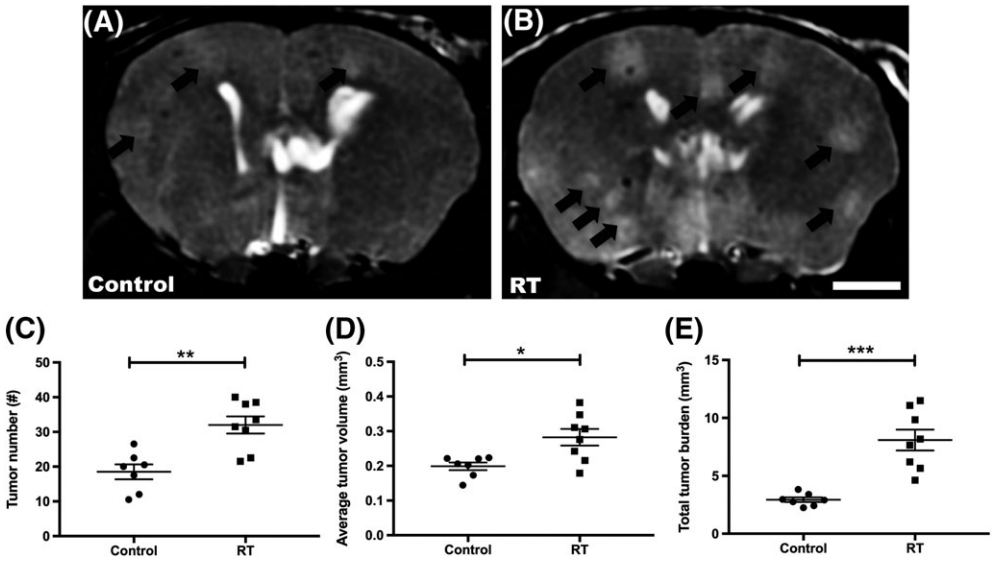

FIGURE 2 Magnetic resonance imaging (MRI) analysis revealed metastatic tumor growth in control A, and pre-irradiated RT; B, mouse brains at endpoint. Black arrows delineate MRI-detectable tumors in representative MR images. Scale bar, 2 mm. RT brains were found to harbor a significantly greater tumor number C, average tumor volume D, and total tumor burden E, than control mouse brains. Analyzed by Student's unpaired two-tailed *t*-test: $^{*}p < 0.05$, $^{**}p < 0.01$, $^{***}p < 0.001$

Image analysis of cell delivery by cellular MRI and analysis of mature metastasis formation by high-resolution anatomical MRI permitted the evaluation of model efficiency between the two conditions. Model efficiency is defined as the proportion of injected cells that successfully arrest in the mouse brain and go on to form MRI-detectable tumors by endpoint. Control and pre-irradiated mouse brain showed the same propensity for cancer cell arrest on the day of intracardiac injection. We observed 1.00 ± 0.16% and 0.99 ± 0.15% of the 20 000 4T1-BR5 cells injected arrested in control and RT brains, respectively (Figure 3A). Despite equivalent cell delivery, 0.16 ± 0.01% of injected cells went on to form MRI-detectable tumors in RT brains, whereas significantly fewer cells (0.09 ± 0.01%) formed mature tumors in non-irradiated control brain (Figure 3B, $p = 0.001$). Thus, a greater proportion ($p = 0.01$) of the arrested cells in RT brains formed metastases by endpoint compared with the control condition (18.1 ± 2.2% *versus* 10.1 ± 1.6% in RT and control brains, respectively; Figure 3C).

3.3 | Effect of pre-irradiation on inflammatory- and metastasis-relevant markers

Endpoint mouse brain sections were stained for several metastasis-relevant pathological markers to initiate assessment of why pre-irradiated neural tissue has a greater propensity for metastatic tumor growth. All stained sections were assessed for percentage positive staining irrespective of staining intensity, as staining by colorimetric methods is easily altered by the length of chromagen exposure and thus intensity is not quantifiable. ICAM-1, a ligand often implicated in the transmigration of cells into tissues, was found to be up-regulated to equivalent levels in both control and pre-RT brain lesions (Figure 4A–C; 14.2 ± 10.1% and 13.0 ± 8.8% tumor area, respectively; $p = 0.4276$).

Our finding that RT brain tumors were of increased size by MRI assessment suggested that a greater proportion of these cells were actively proliferating in the irradiated mouse brain environment. To further examine this suggestion, brain sections were stained for the proliferation marker Ki67 (Figure 4D,E) and both conditions were found to express high percentages of nuclear expression indicative of poor prognosis (>20%).[26] The pre-irradiated brains, however, exhibited tumors with statistically significantly greater Ki67 expression ($p < 0.0001$) than that of control, with 42.4 ± 11.0% and 31.0 ± 10.1% of positive nuclear staining, respectively (Figure 4F).

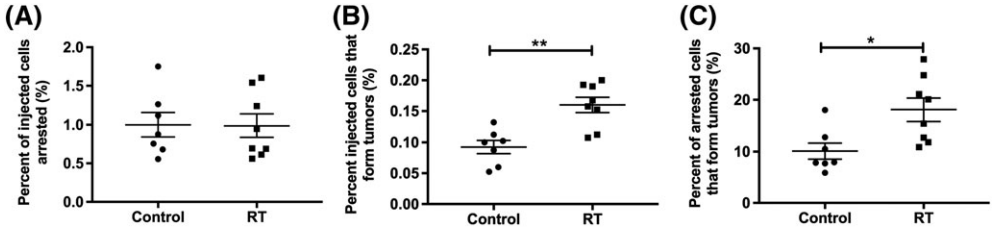

FIGURE 3 Despite statistically equivalent cell delivery A, pre-irradiated (RT) mouse brains exhibited statistically significantly greater efficiency as a greater percentage of injected B, and arrested C, cells successfully formed magnetic resonance imaging (MRI)-detectable tumors by endpoint. Cell delivery was determined by manual void count in cell delivery MR image volumes. Tumor number was determined by the count of delineated tumor boundaries in endpoint MR image volumes. Analyzed by Student's unpaired two-tailed *t*-test: $^{*}p < 0.05$, $^{**}p < 0.01$

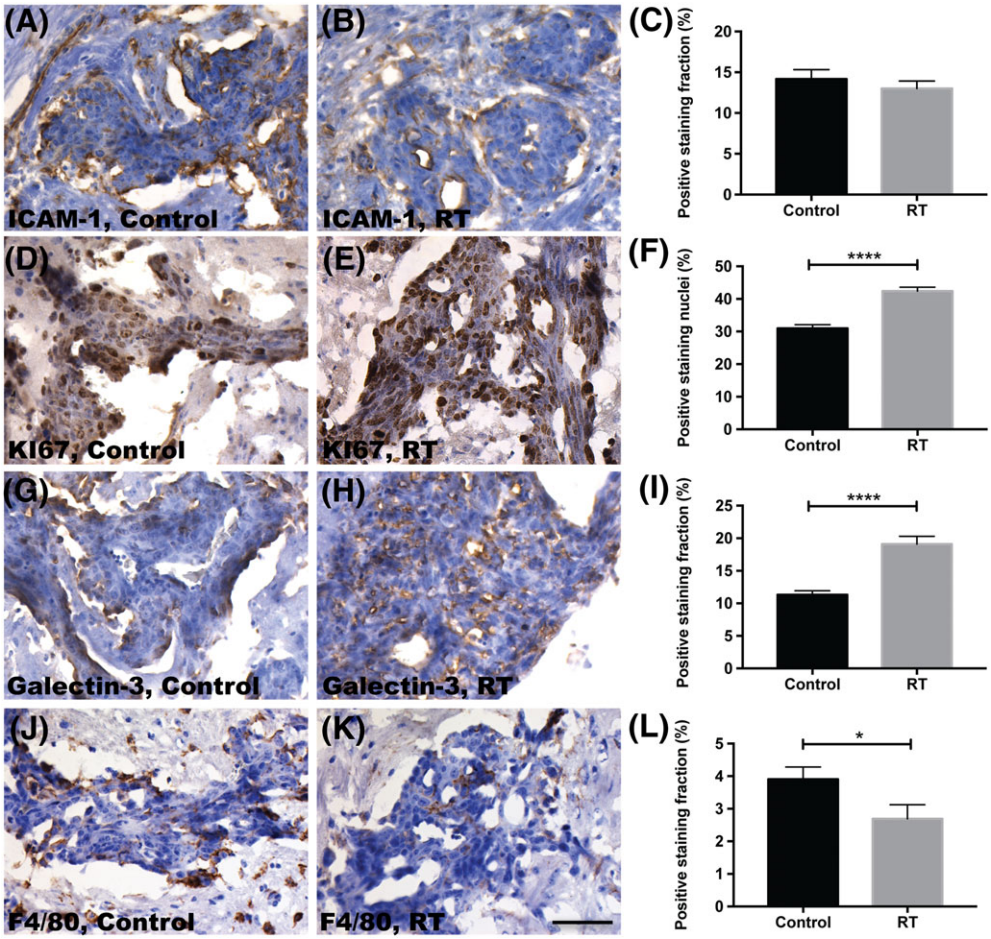

FIGURE 4 Endpoint mouse brain sections were analyzed by immunohistochemistry for differential expression of several metastasis-relevant pathological markers. All stained sections were assessed for percentage positive staining irrespective of staining intensity. Control and pre-irradiated (RT) tumor sections stained equivalently for intercellular adhesion molecule-1 (ICAM-1; A–C). RT brains exhibited tumors with a higher proportion of Ki67 staining nuclei than did non-irradiated controls (D–F). Similarly, more galectin-3 staining was observed in RT brains than in controls (G–I). Control brains showed greater F4/80 staining than RT brains (J–L). All tissue section image analysis data were averaged and analyzed by Student's unpaired two-tailed *t*-test across conditions; $^{*}p < 0.05$, $^{****}p < 0.0001$. Scale bar, 20 μm

Brain sections were also assessed for the expression of galectin-3 (Figure 4G,H), a member of the lectin family that plays an important role in inflammation and has been linked to multiple steps of the metastatic cascade.[27] A significantly greater ($p < 0.0001$, Figure 5I) fraction of tumors grown in pre-irradiated mouse brain stained positively for galectin-3 (19.1 ± 12.7%) than that found in controls (11.3 ± 6.0%). Counter to this finding, staining of sections for the murine macrophage marker F4/80 (Figure 4J,K) was found to be significantly reduced in tumors grown in pre-irradiated neural tissue (Figure 4L, $p = 0.036$).

4 | DISCUSSION

Mouse models have been developed that permit the in-depth evaluation of breast cancer metastasis to the brain and allow the investigation of research questions that cannot be easily addressed in the patient population.[16,28,29] One of these such models, the 4T1-BR5 model, is a relatively new syngeneic mouse model of TNBC brain metastasis.[17,19-22,29,30] Unlike human–mouse xenogeneic models of metastasis, the main advantage of the 4T1-BR5 model is that it permits the evaluation of tumor growth in an immune-competent host environment. The limited work to date with this model has already expanded our knowledge on the blood–tumor barrier,[20,29,30] has helped to identify new therapeutic targets[21,22,30] and has been used to evaluate novel therapeutic strategies.[19,21]

In the present study, we used *in vivo* MRI and endpoint histology to assess the effect of pre-irradiation of brain tissue on the propensity for metastatic tumor growth in the brain. *In vivo* MRI analysis showed that, although cell arrest did not differ between the two conditions, irradiation of neural tissue resulted in the growth of greater numbers and total volume of tumors in the brain. Endpoint histological analysis of these tumors exhibited differential expression of multiple pathological markers linked to proliferation and neural inflammation.

On initiation of this study, our original hypothesis was that RT of the normal mouse brain would trigger inflammation that would promote the arrest of metastatic cancer cells and ultimately lead to the greater formation of brain tumors. Iron cell labeling and high-resolution MRI cell tracking

permitted us to directly address this hypothesis. If increased endpoint tumor burden was the result of an initial promotion of cancer cell arrest in the irradiated brain, a greater proportion of iron-labeled cancer cells would be detected by MRI on the day of cell delivery. This was not the case, as statistically equivalent cell arrest was detected in both conditions. Despite equivalent cell arrest, however, pre-irradiated mouse brains went on to develop greater tumor number and volume at endpoint when compared with non-irradiated controls.

In these types of metastatic models, a subset of the intracardiac-injected cells will successfully arrest in the brain based on cardiac output.[31,32] The majority of arrested cells will disappear from the brain over time, by death or clearance, and only a small subpopulation of arrested cells will form mature MRI-detectable metastases. Heyn et al.[14] used iron-labeled cell delivery and MRI to investigate the cell fate of MDA-MB-231BR (231BR), a related TNBC metastasis model, in normal mouse brain. They found that 94% of arrested cells were transient and lost over time, and only 1.5% were proliferative and formed mature tumors. Our previous work comparing the 231BR and 4T1-BR5 models in normal mouse brain established that the 4T1-BR5 model showed greater efficiency than the 231BR model.[19] The 4T1-BR5 model efficiency, presented in this article, is in agreement with the previously published findings in normal brain. Pre-irradiated mouse brain, however, displayed even greater efficacy in tumor formation, with a significantly greater proportion of injected and arrested cells forming mature tumors at endpoint. This finding suggests that, although cell arrest seems to be unaltered by pre-irradiation of the brain, one or more other stages of the metastatic cascade are favored in irradiated neural tissue. One limitation in our MRI approach is that it did not permit us to determine which stage or stages between cancer cell arrest and mature tumor formation were favored in irradiated neural tissue. One potential tissue change caused by irradiation could have been a breakdown in the blood–brain barrier (BBB). Previous work performed by Lampron et al.[33] looked at the integrity of the BBB in immune-competent mice following 10 Gy of irradiation by staining for blood-derived immunoglobulin G (IgG) and albumin in the neural tissue of control and irradiated mice. Staining patterns were similar for both animal groups, establishing that this level of radiation exposure has not impact on the integrity of the BBB. Even with an intact BBB, it is possible that arrested cells are capable of enhanced extravasation. Alternatively, cells may be better able to survive the irradiated neural microenvironment, have an enhanced ability to establish micrometastases, or have an altered mix of support cells which more effectively reinforce forming tumors. Further experimentation is required to answer these questions; however, we have performed some preliminary endpoint histological assessments to start to evaluate the preferred growth in the irradiated microenvironment.

Our investigation of ICAM-1 found equivalent levels irrespective of brain condition. ICAM-1 expression was elevated in all metastases relative to normal neural tissue. Although others have observed a significant increase in ICAM-1 following irradiation,[5] this ligand has also been linked to the metastatic potential of human breast cancer cell lines,[34] and thus its overexpression within breast cancer metastases was expected. More interestingly, the increased expression of Ki67 in tumors from pre-irradiated mouse brain, coupled with the increase tumor burden found by MRI analysis, indicated more active proliferation of cancer cells within a pre-irradiated microenvironment. Although these data do not specifically identify individual cell types or factors that were altered, they do suggest that cranial irradiation creates an environment that supports the growth of cancer cells.

Our staining analysis also looked at the differential expression of two inflammatory markers in endpoint brain metastases. In another study, Smart et al.[35] examined the neuroinflammatory response within the tumor microenvironment of 231BR tumors following RT. Although all metastatic lesions were surrounded by a zone of activated astrocytes and microglia, the density of either of these cell populations was unaffected by irradiation. Their data suggests that the presence of metastases dictates the neuroinflammatory response independent of radiation exposure. In their study, RT was performed after cell delivery and, in contrast with our findings; the degree of neuroinflammation was similar in metastatic brains with and without radiation treatment. Conversely, we found the differential expression of two inflammatory markers between irradiated and control conditions. In addition to differences in the delivery of RT between the studies, another potential reason for the dissimilarities in our findings may be the immune background of each metastasis model. Although the immune system of the BALB/c mouse used in the 4T1-BR5 model is fully intact, the athymic nude mouse needed for the 231BR model has an inhibited immune system because of its inability to produce T cells.

Persistent neuroinflammation caused by cranial irradiation has been established in immune-competent mouse brain.[4,5,36] Moravan et al.[4] showed that cranial irradiation results in a multiphasic inflammatory response that includes delayed infiltration of immune cells in the brains of immune-competent mice. In C57BL/6 mice, RT resulted in the acute recruitment of neutrophils and the rapid activation of endothelial and glial cell populations. The chronic inflammatory response included the infiltration of T cells and major histocompatibility complex class 2 (MHC II)-positive dendritic cells. MHC II-expressing cells were found to persist at even one full year following RT. In another study, Li et al.[36] looked at the transcriptome of 10 Gy-irradiated microglia cells from both C57BL/6 and BALB/c mice, and revealed similar persistent pro-inflammatory profiles of microglia in both mouse backgrounds for at least 1 month following RT. It has been suggested previously that a subset of microglia becomes M1 polarized following irradiation,[37] and the irradiated transcriptome includes a strong pro-inflammatory component with high expression of cytokines, including interleukin 6 (IL6) and tumor necrosis factor alpha (TNFα).[36] Quite strikingly, a selection of extracellular matrix remodeling enzymes are also significantly up-regulated both 24 h and 1 month following RT. The contributions of such enzymes have already been reported to increase glioma cell migration following irradiation.[38,39]

We were initially surprised by the apparent down-regulation of the murine macrophage marker F4/80 in our pre-irradiated mouse brain sections. As resident activated microglial cells and peripheral macrophages express many of the same surface markers, they are often difficult to differentiate in disease models. To circumvent this issue, Morganti et al.[5] employed a smart approach in their investigation of the effect of cranial irradiation on the induced inflammatory response in the brain. In their study, macrophages and microglial cells expressed different fluorescent markers that enabled their differentiation. They found that the brain's innate immune response was very vulnerable to cranial RT and displayed a transient, but persistent, decrease in microglia following radiation exposure. RT was also sufficient to induce the migration of peripherally derived

macrophages into the brain, and was suggested to be an attempt at replacing depleted resident microglia. Others have shown that selective depletion in resident microglia results in the recruitment, infiltration and engraftment of peripheral macrophages into the brain.[36,40] Thus, it is possible that the reduction in F4/80 staining observed in our experimental tumors may be the result of the depletion of microglia caused by our radiation treatment, although further investigation is necessary to confirm this hypothesis.

Quite interestingly, work in rat models of primary brain cancer have also shown an increased propensity for tumor growth in irradiated brain, which presented as increased infiltrative growth and reduced median survival in experimental animals.[41-43] These studies have shown enduring effects of irradiation on rat cell lines and neural tissue, including prolonged enhanced expression of matrix metalloproteinases in irradiated glioma cells[41] and up-regulation of inflammatory cytokines and pro-infiltration molecules in irradiated neural tissue.[42] More recently, Desmarais et al.[43] have shown that treatment with a cyclooxygenase-2 (COX-2) inhibitor can help circumvent glioma cell infiltration in irradiated rat brain, and have identified it as a good candidate as adjuvant to RT. Mitigating interleukin-1β, a pro-infiltration mediator implemented in neural irradiation, has also been identified as a candidate therapeutic target. Continued work in preclinical models of primary and metastatic brain tumors will be fundamental for the evaluation of ideal treatment protocols and improved patient outcomes.

5 | CONCLUSION

RT is routinely used in the treatment of many different types of cancer, often in combination with surgery or chemotherapy. In many situations, large amounts of healthy tissue receive significant doses of RT, causing detrimental side effects, including cognitive deficits and prolonged inflammation. For brain metastases of breast cancer, the whole brain is treated with RT for patients with multiple brain metastases. Our results have shown that RT of normal neural tissue results in the promotion of metastatic tumor growth in the brain. These preclinical data suggest an increased risk that may be relevant to subpopulations of patients with brain tumors, particularly those with residual systemic disease or with residual radioresistant brain cancer. With these initial findings, our future investigations will include a deeper inquiry into the differential timeframes and fractionated RT dose delivery. Also, as RT is an indispensable tool in the fight against brain tumor progression, our next research steps will include further mechanistic assessment of the risk, as well as the evaluation of potential adjunct therapies to mitigate metastasis progression in irradiated normal brain.

ACKNOWLEDGEMENTS

This research was supported by grants from the Canadian Institutes of Health Research and the Brain Tumour Foundation of Canada.

ORCID

Amanda M. Hamilton http://orcid.org/0000-0002-2960-9771

REFERENCES

1. Breast LNU. cancer brain metastases: new directions in systemic therapy. *Ecancermedicalscience*. 2013;7:307.
2. Niikura N, Hayaski N, Masuda N, et al. Treatment outcomes and prognostic factors for patients with brain metastases from breast cancer of each subtype: a multicenter retrospective analysis. *Breast Cancer Res Treat*. 2014;147:103-112.
3. Arvold ND, Oh KS, Niemierko A, et al. Brain metastases after breast-conserving therapy and systemic therapy: incidence and characteristics by biologic subtype. *Breast Cancer Res Treat*. 2012;136:153-160.
4. Moravan MJ, Olschowka JA, Williams JP, O'Banion MK. Cranial irradiation leads to acute and persistent neuroinflammation with delayed increases in T-cell infiltration and CD11c expression in C57Bl/6 mouse brain. *Radiat Res*. 2011;176(4):459-473.
5. Morganti JM, Jopson TD, Liu S, Gupta N, Rosi S. Cranial irradiation alters the brain's microenvironment and permits $CCR2^{+}$ macrophage infiltration. *PLoS One*. 2014;9(4):e93650.
6. Condeelis J, Pollard JW. Macrophages: obligate partners for tumor cell migration, invasion, and metastasis. *Cell*. 2006;124:263-266.
7. Qian LW, Mizumoto K, Urashima T, et al. Radiation-induced increase in invasive potential of human pancreatic cancer cells and its blockade by a matrix metalloproteinase inhibitor, CGS27023. *Clin Cancer Res*. 2002;8:1223-1227.
8. Wild-Bode C, Weller M, Wick W. Molecular determinants of glioma cell migration and invasion. *J Neurosurg*. 2001;94:978-984.
9. Rofstad EK, Mathiesen B, Galappathi K. Increased metastatic dissemination in human melanoma xenografts after subcurative radiation treatment: radiation-induced increase in fraction of hypoxic cells and hypoxia-induced up-regulation of urokinase-type plasminogen activator receptor. *Cancer Res*. 2004;64:13-18.
10. Kaliski A, Maggiorella L, Cengel KA, et al. Angiogenesis and tumor growth inhibition by a matrix metalloproteinase inhibitor targeting radiation-induced invasion. *Mol Cancer Ther*. 2005;4:1717-1728.
11. Speake WJ, Dean RA, Kumar A, Morris TM, Scholefield JH, Watson SA. Radiation induced MMP expression from rectal cancer is short lived but contributes to in vitro invasion. *Eur J Surg Oncol*. 2005;31:869-874.
12. Wang JL, Sun Y, Wu S. Gamma-irradiation induces matrix metalloproteinase II expression in a p53-dependent manner. *Mol Carcinog*. 2000;27:1105-1116.
13. Bouchard G, Bouvette G, Therriault H, Bujold R, Saucier C, Paquette B. Pre-irradiation of mouse mammary gland stimulates cancer cell migration and development of lung metastases. *Br J Cancer*. 2013;109:1829-1838.

14. Heyn C, Ronald JA, Ramadan SS, et al. In vivo MRI of cancer cell fate at the single-cell level in a mouse model of breast cancer metastasis to the brain. *Magn Reson Med*. 2006;56(5):1001-1010.
15. Ribot EJ, Martinez-Santiesteban FM, Simedrea C, et al. In vivo single scan detection of both iron-labeled cells and breast cancer metastases in the mouse brain using balanced steady-state free precession imaging at 1.5T. *J Magn Reson Imaging*. 2011;34(1):231-238.
16. Murrell DH, Foster PJ, Chambers AF. Brain metastases from breast cancer: lessons from experimental magnetic resonance imaging studies and clinical implications. *J Mol Med (Berl)*. 2014;92:5-12.
17. Hamilton AM, Aidoudi-Ahmed S, Sharma S, et al. Nanoparticles coated with the tumor-penetrating peptide iRGD reduce experimental breast cancer metastasis in the brain. *J Mol Med (Berl)*. 2015;8(3):176-184.
18. Murrell DH, Zarghami N, Jensen MD, et al. MRI surveillance of cancer cell fate in a brain metastasis model after early radiotherapy. *Magn Reson Med*. 2016;2:3-6.
19. Hamilton AM, Foster PJ. In vivo magnetic resonance imaging investigating the development of experimental brain metastases due to triple negative breast cancer. *Clin Exp Metastasis*. 2017;34(2):133-140.
20. Lockman PR, Mittapalli RK, Taskar KS, et al. Heterogeneous blood–tumor barrier permeability determines drug efficacy in experimental brain metastases of breast cancer. *Clin Cancer Res*. 2010;16(23):5664-5678.
21. Fitzgerald DP, Subramanian P, Deshpande M, et al. Opposing effects of pigment epithelium-derived factor on breast cancer cell versus neuronal survival: implication for brain metastasis and metastasis-induced brain damage. *Cancer Res*. 2012;72(1):144-153.
22. Woditschka S, Evans L, Duchnowska R, et al. DNA double-strand break repair genes and oxidative damage in brain metastasis of breast cancer. *J Natl Cancer Inst*. 2014;106(7):145.
23. McFadden C, Mallett CL, Foster PJ. Labeling of multiple cell lines using a new iron oxide agent for cell tracking by MRI. *Contrast Media Mol Imaging*. 2011;6(6):514-522.
24. Jensen MD, Hrinivich WT, Jung JA, et al. Implementation and commissioning of an integrated micro-CT/RT system with computerized independent jaw collimation. *Med Phys*. 2013;40(8):13.
25. Percy DB, Ribot EJ, Chen Y, et al. vivo characterization of changing blood–tumor barrier permeability in a mouse model of breast cancer metastasis: a complementary magnetic resonance imaging approach. *Invest Radiol*. 2011;46(11):718-725.
26. Stuart-Harris R, Caldas C, Pinder SE, Pharoah P. Proliferation markers and survival in early breast cancer: a systematic review and meta-analysis of 85 studies in 32,825 patients. *Breast*. 2008;17(4):323-334.
27. Shin T. The pleiotropic effects of galectin-3 in neuroinflammation: a review. *Acta Histochem*. 2013;115(5):407-411.
28. Daphu I, Sundstrom T, Horn S, et al. In vivo animal models for studying brain metastases: value and limitations. *Clin Exp Metastasis*. 2013;30(5):695-710.
29. Adkins CE, Mohammad AS, Terrell-Hall TB, et al. Characterization of passive permeability at the blood–tumor barrier in five preclinical models of brain mestatases of breast cancer. *Clin Exp Metastasis*. 2016;33(4):373-383.
30. Bohn KA, Adkins CE, Nounou MI, Lockman PR. Inhibition of VEGF and angiopoietin-2 reduce brain metastases of breast cancer burden. *Front Pharmacol*. 2017;8:193.
31. Quintana A, Raczka E, Bonaccorsi A. Cardiac output distribution measured with radioactive microspheres in the mouse. *Pharmacol Res Commun*. 1979;11(3):245-252.
32. Basse P, Hokland P, Heron I, Hokland M. Fate of tumor cells injected into left ventricle of heart in BALB/c mice: role of natural killer cells. *J Natl Cancer Inst*. 1988;80(9):657-665.
33. Lampron A, Lessard M, Rivest S. Effects of myeloablation, peripheral chimerism, and whole-body irradiation on the entry of bone marrow-derived cells into the brain. *Cell Transplant*. 2012;21:1149-1159.
34. Rosette C, Roth RB, Oeth P, et al. Role of ICAM1 in invasion of human breast cancer cells. *Carcinogenesis*. 2005;26(5):943-950.
35. Smart D, Garcia-Glaessner A, Palmieri D, et al. Analysis of radiation therapy in a model of triple-negative breast cancer metastasis. *Clin Exp Metastasis*. 2015;32:717-727.
36. Li MD, Burns TC, Kumar S, Morgan AA, Sloan SA, Palmer TD. Aging-like changes in the transcriptome of irradiated microglia. *Glia*. 2015;63:754-767.
37. Hua K, Schindler MK, McQuail JA, Forbes ME, Riddle DR. Regionally distinct responses of microglia and glial progenitor cells to whole brain irradiation in adults and aging rats. *PLoS One*. 2012;7:e52728.
38. Kesanakurti D, Chetty C, Rajasekhar Maddirela D, Gujrati M, Rao JS. Essential role of cooperative NF-kappaB and Stat3 recruitment to ICAM-1 intronic consensus elements in the regulation of radiation-induced invasion and migration in glioma. *Oncogene*. 2013;32:4144-5155.
39. Shankar A, Kumar S, Iskander A, et al. Subcurative radiation significantly increases proliferation, invasion and migration of primary GBM in vivo. *Chin J Cancer*. 2013;33:148-158.
40. Varvel NH, Grathwohl SA, Baumann F, et al. Microglial repopulation model reveals a robust homeostatic process for replacing CNS myeloid cells. *Proc Natl Acad Sci U S A*. 2012;109(44):18150-18155.
41. Wild-Bode C, Weller M, Rimner A, Dichgans J, Wick W. Sublethal irradiation promotes migration and invasiveness of glioma cells: implications for radiotherapy of human glioblastoma. *Cancer Res*. 2001;61:2744-2750.
42. Desmarais G, Fortin D, Bujold R, Wagner R, Mathieu D, Paquette B. Infiltration of glioma cells in brain parenchyma stimulated by radiation in the F98/Fischer rat model. *Int J Radiat Biol*. 2012;88(8):565-574.
43. Desmarais G, Charest G, Fortin D, Bujold R, Mathieu D, Paquette B. Cyclooxygenase-2 inhibitor prevents radiation-enhanced infiltration of F98 glioma cells in brain of Fischer rat. *Int J Radiat Biol*. 2015;91(8):624-633.

How to cite this article: Hamilton AM, Wong SM, Wong E, Foster PJ. Cranial irradiation increases tumor growth in experimental breast cancer brain metastasis. *NMR in Biomedicine*. 2018;31:e3907. https://doi.org/10.1002/nbm.3907